

PAPER

Underwater acoustic metamaterial based on double Dirac cone characteristics in rectangular phononic crystals^{*}

To cite this article: Dong-Liang Pei *et al* 2019 *Chinese Phys. B* **28** 124301

View the [article online](#) for updates and enhancements.

Recent citations

- [Realization of terahertz single-band metamaterial filter based on the bright-bright coupling](#)
Min Zhong

Underwater acoustic metamaterial based on double Dirac cone characteristics in rectangular phononic crystals*

Dong-Liang Pei(裴东亮)^{1,2}, Tao Yang(杨洮)^{1,2}, Meng Chen(陈猛)^{1,2,†}, and Heng Jiang(姜恒)^{1,2,‡}

¹Key Laboratory of Microgravity, Institute of Mechanics, Chinese Academy of Sciences, Beijing 100190, China

²University of Chinese Academy of Sciences, Beijing 100049, China

(Received 11 October 2019; revised manuscript received 4 November 2019; published online 29 November 2019)

We theoretically construct a rectangular phononic crystal (PC) structure surrounded by water with C_{2v} symmetry, and then place a steel rectangular scatterer at each quarter position inside each cell. The final complex crystal has two forms: the vertical type, in which the distance s between the center of the scatterer and its right-angle point is greater than $0.5a$, and the transverse type, in which s is smaller than $0.5a$ (where a is the crystal constant in the x direction). Each rectangular scatterer has three variables: length L , width D , and rotation angle θ around its centroid. We find that, when L and D change and θ is kept at zero, there is always a linear quadruply degenerate state at the corner of the irreducible Brillouin zone. Then, we vary θ and find that the quadruply degenerate point splits into two doubly-degenerate states with odd and even parities. At the same time, the band structure reverses and undergoes a phase change from topologically non-trivial to topologically trivial. Then we construct an acoustic system consisting of a trivial and a non-trivial PC with equal numbers of layers, and calculate the projected band structure. A helical one-way transmission edge state is found in the frequency range of the body band gap. Then, we use the finite-element software Comsol to simulate the unidirectional transmission of this edge state and the backscattering suppression of right-angle, disorder, and cavity defects. This acoustic wave system with rectangular phononic crystal form broadens the scope of acoustic wave topology and provides a platform for easy acoustic operation.

Keywords: double Dirac cone, topological edge state, rectangular phononic crystal, topological phase transition

PACS: 43.30.+m, 43.20.+g, 42.70.Qs

DOI: 10.1088/1674-1056/ab55d2

1. Introduction

The discovery of the quantum spin Hall effect not only opened a new chapter in condensed matter physics^[1–5] but also brought the mathematical concept of topology into physical systems. Topological states have many special features,^[6–10] such as the edge states of unidirectional transmission and backscatter suppression that is insensitive to defects. Some researchers break the time-reversal symmetry of optoelectronic systems by applying a magnetic field to form topological states of unidirectional transmission on the edges of non-trivial and trivial structures.^[11–14] Photonic and phononic crystals (PCs) are highly similar to electron systems in terms of band structures and Bloch's law, whereby they can also achieve topological states similar to quantum systems.^[15–17] An acoustic system belongs to the Bose subsystem, which is essentially different from an electromagnetic system. Therefore, it is impossible to break the time-reversal symmetry of an acoustic system using a magnetic field.

Accordingly, some researchers have mimicked the symmetry of a magnetic field in acoustic systems by introducing

a rotating airflow or an acoustic pseudospin to form acoustic edge states.^[18,19] Some have used the classical graphene model of an electronic system to construct a two-dimensional structure with C_{3v} symmetry in an acoustic system, thus forming a degenerate Dirac cone at the corner of the Brillouin zone, and then rotated the scatterer. Reducing the symmetry of the structure to C_3 opens the Dirac cone to form a band gap.^[20–26] Lu *et al.* constructed a three-layer structure similar to a sandwich with multiple single-layer structures with different topological phases, realizing an edge state with topological valley properties.^[20] Xia *et al.* designed a photonic crystal that simultaneously exhibits the topological states of sound and light using cylindrical spacing of different diameters.^[27] By adjusting the impedance ratio between the cylindrical scatterer and the matrix in the honeycomb crystals, they found a Dirac cone and a double Dirac cone at different degenerate points of the structure. By reducing the symmetry of the structure (from C_{6v} to C_{3v}), the authors simultaneously implemented the topological edge transmission of sound and light.

Early studies focused on the corner point or center points

*Project supported by the National Natural Science Foundation of China (Grant Nos. 11602269, 11972034, and 11802213), the Strategic Priority Research Program of the Chinese Academy of Sciences (Grant No. XDB22040301), and the Research Program of Beijing, China (Grant Nos. Z161100002616034 and Z171100000817010).

†Corresponding author. E-mail: chenmeng@imech.ac.cn

‡Corresponding author. E-mail: hengjiang@imech.ac.cn

© 2019 Chinese Physical Society and IOP Publishing Ltd

<http://iopscience.iop.org/cpb> <http://cpb.iphy.ac.cn>

of the Brillouin zone. Later, researchers discovered that a Dirac point can also exist at the edge of the Brillouin zone.^[28] For example, researchers found that increasing the ratio of the scatterer of a rectangular PC moves the Dirac point from the midpoint of the edge to the corner. Some have further proposed a doubly degenerate point in a square crystal and found a topological phase transition by adjusting the rotation angle of the scatterer.^[29] Then the author constructed a "back" shape acoustic model and demonstrated its topological edge state and topological angle state. However, no study has been done on the edge state properties of rectangular PCs with double dirac cone.

This paper models a PC structure with rectangular cells placed in water. A rectangular scatterer is placed at each of the four quarter positions of each cell, and the phononic band structure is studied by changing the following variables of each scatterer: its length L , width D , and rotation angle θ around its centroid. We find that when $\theta = 0$, there is always a quadruply degenerate point at the corner M of the irreducible Brillouin zone, but its value changes as L and D change. Changing θ splits the four simple points and causes the system to undergo a topological phase transition. Then, using the finite-element simulation software Comsol, we find that the edge structure constructed by topologically trivial and nontrivial PCs is robust to right-angle, disorder, and cavity defects.

2. Rectangular acoustic system

We study a two-dimensional crystal in water with rectangular cells, as shown in Fig. 1. The crystal constant in the x direction is $a = 10$ mm, and that in the y direction is $b = 2a$. An identical steel rectangular scatterer is placed at each of the four quarter positions of each unit: $(a/4, a/2)$, $(a/4, -a/2)$, $(-a/4, -a/2)$, and $(-a/4, a/2)$. When changing either L , D , or θ , the mirror symmetry of the entire cell is maintained. The cell basis vectors are $\mathbf{a}_1 = a\hat{i}$ and $\mathbf{a}_2 = 2a\hat{j}$. The acoustic wave equation for propagation in such a system is

$$\nabla \cdot \left(\frac{\nabla p}{\rho_r(x)} \right) = -\frac{\omega^2}{c_0^2} \frac{p}{B_r(x)}, \quad (1)$$

where p is the sound pressure field in space, ρ_r and B_r respectively represent the mass density and body modulus of the acoustic propagation medium relative to the aqueous medium, ω is the angular frequency, and $c_0 = 1530$ m/s is the speed of sound in water. Each steel scatterer has a density of 7800 kg/m³, and the longitudinal wave velocity is 5650 m/s. The effect of sound propagation in the scatterer is ignored be-

cause the impedances of water and steel differ greatly, and the steel column is treated as a rigid body.

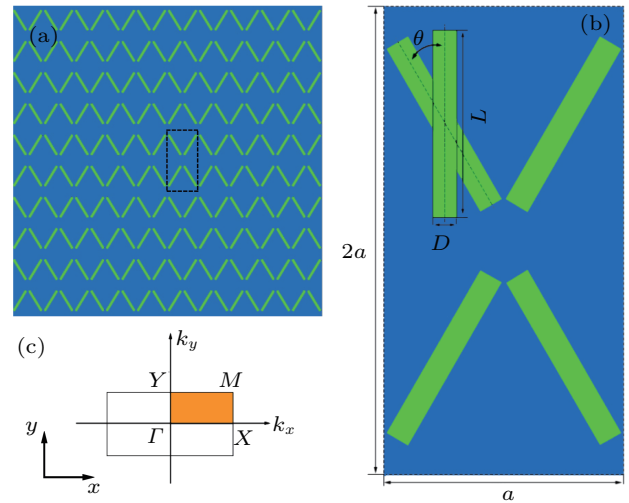


Fig. 1. (a) PC consisting of rectangular scatterers surrounded by water positioned in a rectangular lattice. (b) Cell of a rectangular PC. (c) Irreducible Brillouin zone of a cell.

The distance s from the center of the scatterer to its right-angle point is

$$s = \sqrt{D^2 + L^2}/2. \quad (2)$$

For scatterers with s greater than $0.5a$, the maximum rotation angle is

$$\theta = \arctan\left(\frac{L}{D}\right) - \arccos\left(\frac{a}{2\sqrt{D^2 + L^2}}\right), \quad \theta < 90^\circ. \quad (3)$$

For a scatterer with s smaller than $0.5a$, the angle of rotation is $\pm 180^\circ$. Then, keeping θ at zero and varying L and D , we study the band structure and frequency variation at the corner M of the irreducible Brillouin zone. It can be seen from Fig. 2(a) that when D is fixed, the frequency at M decreases as L increases. To further understand this variation, figure 2(b) shows a case with $D = 0.1a$, and the frequency at M monotonically decreases in the form of a nearly straight line as L increases. At the same time, it can also be seen from Fig. 2(a) that when L is in the range of $0.4a-0.8a$, the frequency at M decreases slightly as D increases, and then increases slowly. In Fig. 2(c), L takes $0.48a$. When D increases from $0.04a$ to $0.46a$, the frequency decreases from 72200 Hz at $D = 0.04a$ to 71700 Hz at $0.1a$, and then gradually increases to 76300 Hz at $0.46a$.

Next, we will study two cases with different s of the scatterer, as shown by points A and B in Fig. 2(a). The rotation angle θ of case A is $\pm 180^\circ$, which is called T (transverse) type. The maximum rotation angle θ of case B is $\pm 31^\circ$, which is called V (vertical) type.

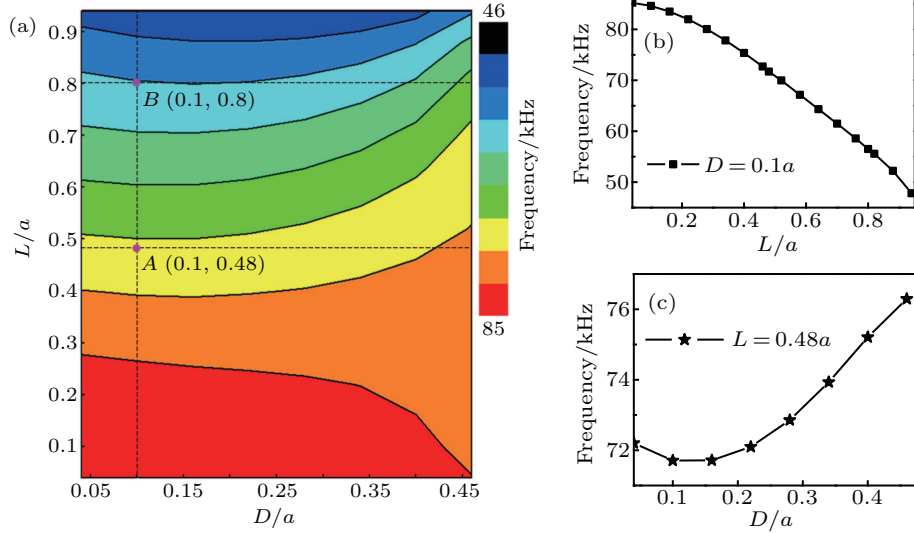


Fig. 2. (a) Frequency of the quadruply degenerate state at the corner M of the Brillouin zone as a function of scatterer width D and length L . (b) When $D = 0.1a$, the frequency of M changes with L . (c) When $L = 0.48a$, the frequency of M changes with D .

3. The $k \cdot p$ perturbation analysis of the system

In order to study the dispersion relation near the point M , we transform the acoustic wave equation into an eigenvalue problem

$$H\psi_{n,\mathbf{k}}(\mathbf{r}) = \omega_{n,\mathbf{k}}^2 \kappa^{-1}(\mathbf{r}) \psi_{n,\mathbf{k}}(\mathbf{r}), \quad (4)$$

where $H = -\nabla \cdot [\rho^{-1}(\mathbf{r}) \nabla]$ is the system Hamiltonian, and $\psi_{n,\mathbf{k}}$ and $\omega_{n,\mathbf{k}}$ are the sets of wave functions and characteristic frequencies of the Bloch wave vector in the n -th band, respectively. According to the $\mathbf{k} \cdot \mathbf{p}$ perturbation theory,^[30–34] the wave function at one wave vector can be represented by a linear combination of wave functions at the near-wave vector \mathbf{q} around it. Therefore, \mathbf{q} is considered to be small here. The theoretical Hamiltonian of the system is

$$H_{nn'} = \omega_n^2 \delta_{nn'} + \mathbf{q} \cdot \mathbf{P}_{nn'} + \dots, \quad (5)$$

where ω_n is the characteristic frequency in the n -th band at the degenerate point. Only the first-order term of \mathbf{q} is used in the formula, and higher-order terms are omitted. The matrix term is expressed as

$$\mathbf{P}_{nn'} = \int_{\text{u.c.}} \psi_{n,\mathbf{k}}^*(\mathbf{r}) \{ -i [2\rho^{-1}(\mathbf{r}) \nabla + \nabla \rho^{-1}(\mathbf{r})] \} \psi_{n',\mathbf{k}}(\mathbf{r}) d\mathbf{r}. \quad (6)$$

If two states of the sound pressure field at a certain point have odd parity, the other two states have even parity. Other acoustic frequencies are farther away from the degeneracy point. According to the perturbation theory, we can only consider the contribution of the two double degenerate states at this point. Then, \mathbf{q} can be expressed on the basis ($|s\rangle, |d\rangle, |p_x\rangle, |p_y\rangle$) as

$$q_x P_x + q_y P_y = \begin{pmatrix} 0 & 0 & a q_x & b q_y \\ 0 & 0 & c q_y & d q_x \\ a^* q_x & b^* q_y & 0 & 0 \\ c^* q_y & d^* q_x & 0 & 0 \end{pmatrix}. \quad (7)$$

Analysis of the slip symmetry of the applied structure then results in a linear quadruply degenerate state at this point.

4. Band structure and topological phase transition

Now we change the third scatterer variable θ , and find that the double Dirac cone appears open or closed as θ varies; that is, a topological phase transition of the structure occurs. Figure 3 shows the band structure and topological phases of the V- and T-type structures, revealing the change from non-trivial to trivial as the rotation angle of the scatterer changes. Figure 3(a) is the band structure of a V-type PC with four linear quadruply degenerate points at M for $\theta = 0^\circ$. On the left side, $\theta = -20^\circ$, and M is divided into two doubly degenerate points, where the low frequency is the q state with even parity and the high frequency is the p state with odd parity. On the right side, $\theta = 20^\circ$, and the band structure and band gap frequency are the same as those for $\theta = -20^\circ$, but the sound pressure distribution at M is opposite; that is, the low frequency is the p state while the high frequency is the q state. Figure 3(b) further shows the variation of the q and p states with the rotation angle. When θ increases from -30° to 0° , the bandwidth at M gradually decreases. In this angular range, the q state is always below the p state; the system is in a non-trivial state. At $\theta = 0$, the q and p states coincide and the system is in a quadruply degenerate state. When θ increases from 0° to 30° , the bandwidth at M increases gradually. In this angular range, the q state is always above the p state; the system is in a trivial state. Therefore, figures 3(a) and 3(b) show that the system undergoes a transition from a non-trivial to a trivial phase as θ changes from negative to positive. Figure 3(c) shows the band structure of a T-type PC, which is similar to the V-type one, with a linear quadruply degenerate point at M for $\theta = 0$. When $\theta = -60^\circ$ and 60° , the band structures are the same, but the frequencies of the q and p states are opposite. When θ increases from -90° to 0° , the bandwidth at M increases

first and then decreases to 0. In this angular range, the q state is always below the p state, so the system is in a non-trivial state. When θ increases from 0° to 90° , the bandwidth at M increases first and then decreases to 0. In this angular range,

the q state is always above the p state, so the system is in a trivial state. Therefore, the T-type system also undergoes a phase transition from non-trivial to trivial as θ changes from negative to positive.

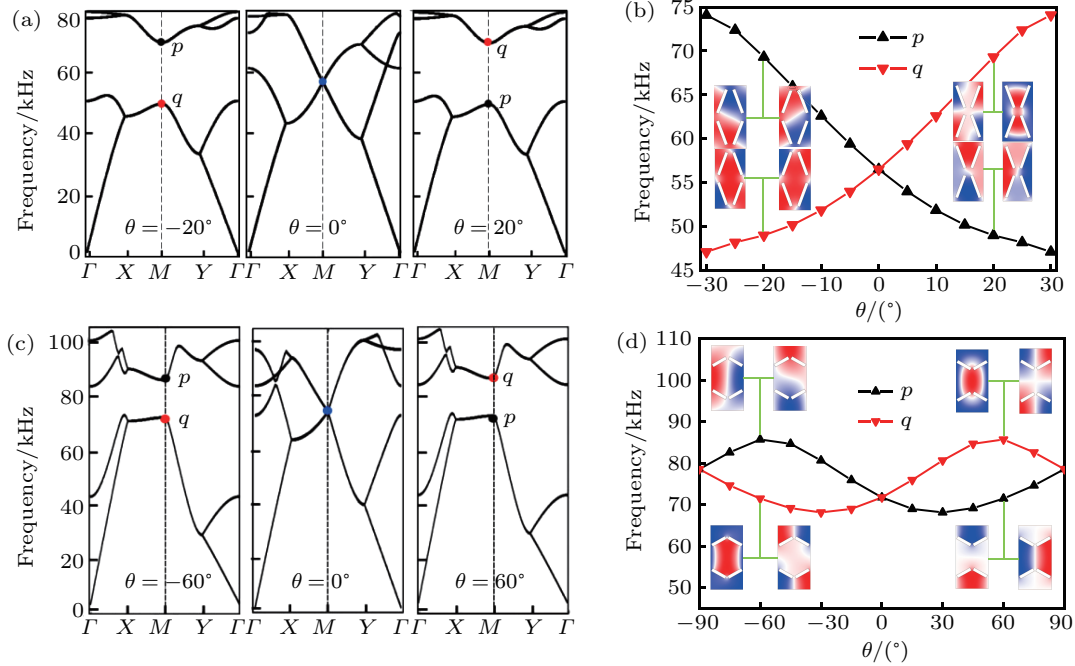


Fig. 3. (a) Band structure of a V-type PC when θ is -20° , 0° , and 20° respectively. (b) Variation of q and p states with rotation angle θ increasing from -30° to 30° , the inset shows the distribution of sound pressure of q and p states when $\theta = \pm 20^\circ$. (c) Band structure of a T-type PC when θ is -60° , 0° , and 60° respectively. (d) Variation of q and p states with θ increasing from -90° to 90° for the T-type PC, the inset shows the distribution of sound pressure of q and p states when $\theta = \pm 60^\circ$.

5. Topological edge state

From the perturbation analysis of the system and the phase diagram of its topology, we find that the two PC types proposed in this paper are similar to a system with a quantum spin Hall effect, so the V and T sound waves should have an acoustic spin Hall effect. Accordingly, we use topologically trivial and non-trivial PCs to splice in the x and y directions. Then, we analyze the projection bands of the spliced structure in the corresponding direction. We splice a 10-layer topologically trivial V-type PC with $\theta = -20^\circ$ and a 10-layer topologically non-trivial V-type PC with $\theta = 20^\circ$ along the x and y directions. We also splice a 10-layer trivial T-type PC with $\theta = -60^\circ$ and a 10-layer non-trivial T-type PC with $\theta = 60^\circ$. The result is shown in Fig. 4. The gray area in Fig. 4(a) represents the bulk state of the spliced structure, the red dotted line represents the edge state existing in the band gap, and the four illustrations represent the sound pressure distribution of the edge state at different positions. The black arrows represent the direction of energy flow. We can see from Fig. 4(a) that when $k_x = 0.96\pi/a$, the energy at the low-frequency point flows clockwise downward, and the energy at the high-frequency point flows counterclockwise. When $k_x = 1.04\pi/a$, the energy at the low-frequency point flows

counterclockwise, and the energy at the high-frequency point flows clockwise downward, opposite to the direction of the energy flow at $0.96\pi/a$. The other three boundary states show the similar phenomenon. The boundary state shapes and bandwidths are slightly different for the different splices of the V- and T-type PCs. Therefore, if the two boundaries are concentrated into one structure, such as the Z-shaped boundary shown in the text below, the frequency range through which sound waves can pass should be the intersection of the two boundary state bands.

The topological edge is different from an ordinary edge. It is immune to corner, cavity, and disorder defects, and can ensure that the incident sound wave propagates smoothly along the edge without reflection. We simulate a plane wave incident from the left side into a hydroacoustic region consisting of 20×15 hybrid PCs with topological edges (Fig. 5). The area is composed of a V-type trivial PC with $\theta = -20^\circ$ and a non-trivial PC with $\theta = 20^\circ$, and contains two right-angled Z-shapes, as shown in Fig. 5(a). Figure 5(b) shows the addition of cavity and disorder defects on the basis of Fig. 5(a). We can see from Figs. 5(a) and 5(b) that the sound waves propagate without reflection along the edge, and the sound pressure of the transmitted wave is hardly affected. Figures 5(c) and 5(d) show the Z-shaped edge composed of a T-type trivial

PC with $\theta = 60^\circ$ and -60° . Injecting an acoustic wave with $f = 79.5$ kHz into the left side yields a similar phenomenon to that of the V-shaped structure. Therefore, both V-type T-type

topological edges have good immunity to right angle, cavity, and disorder, and sound waves can bypass these defects and continue to propagate without reflection.

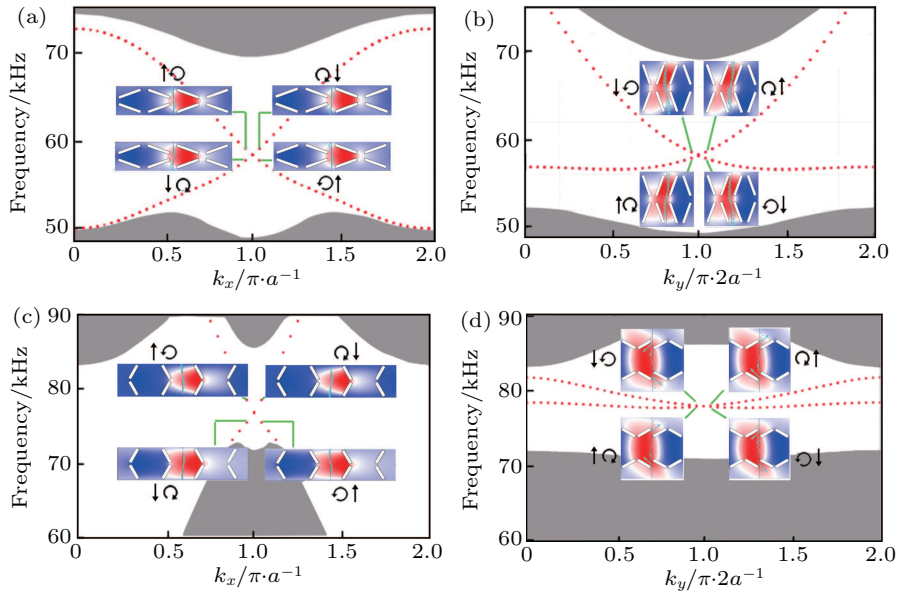


Fig. 4. Projection band structure of V- and T-type PCs. Panels (a) and (b) are projection band structures of a spliced structure of a V-shaped phononic crystal with $\theta = 20^\circ$ and -20° (10 layers each) in the x and y directions, respectively. The gray area indicates the bulk state, and red dotted line indicates the edge state. Panels (c) and (d) are projection band structures of a spliced structure of a T-type phononic crystal with $\theta = 60^\circ$ and -60° (10 layers each) in the x and y directions, respectively. The illustrations in (a)–(d) show the distributions of sound pressure around the splicing boundary at different wave vectors. The black arrows represent the energy flow directions.

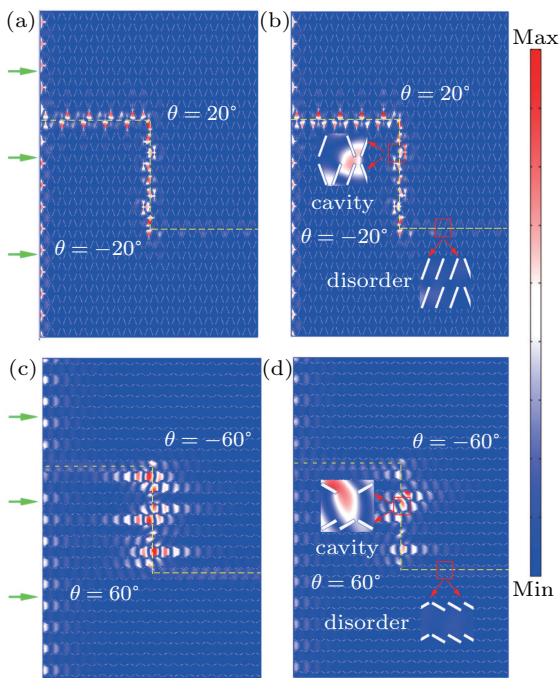


Fig. 5. (a) and (b) Field pattern of V-type edge simulated at 68 kHz without and with defects, respectively. (c) and (d) Field pattern of T-type edge simulated at 79.5 kHz without and with defects, respectively. The green arrow indicates that the plane wave is incident from the left side.

6. Conclusion

This study has theoretically constructed a rectangular PC with C_{2v} symmetry and placed four steel rectangular scatterers at each quarter position inside the crystal. The final composite

crystal has two different forms: the V-type, where the distance between the center point of the scatterer and its right-angle point, s , is greater than $0.5a$, and the T-type, where s is smaller than $0.5a$. We found a quadruply degenerate state when the length L and width D of the scatterer are varied at $\theta = 0$. This quadruply degenerate state consists of two odd-parity degenerate states and two even-parity states at the corner M and the sliding symmetry of the structure, the perturbation method was used to calculate the effective Hamiltonian of the structure and the linear degeneracy of the band at the quadruply degenerate point. We also found that when D is fixed, the frequency at M decreases with increasing L ; when L is in the range $0.4a$ – $0.8a$, the frequency at M first decreases slightly as D increases and then increases. By changing θ , we found that the quadruply degenerate state splits into two doubly degenerate states, and the band structure reverses as θ changes from negative to positive. Then, we spliced the systems with trivial and nontrivial states along the x and y directions and calculated the projection band structures. We found a one-way transmission edge of the “spin–momentum” locking in the frequency range of the body band gap. The finite-element software Comsol was then used to simulate the acoustic reflection of a Z-shaped edge consisting of two right angles composed of 20×15 PCs, and we found that the sound waves could propagate without reflection along the edge. Then, we intro-

duced disorder and cavity defects to the edge, and found that the sound wave can still propagate around these defects. This shows the backscattering suppression of the topological edge.

The topological PC composed of steel rectangular scatterers surrounded by water is simple and practical, and can realize stable underwater acoustic wave edge transmission with good performance. This has potential application to underwater acoustic communication.

References

- [1] Bernevig B A, Hughes T L and Zhang S C 2006 *Science* **314** 1757
- [2] Kane C L and Mele E J 2005 *Phys. Rev. Lett.* **95** 226801
- [3] Yang W, Chang K and Zhang S C 2008 *Phys. Rev. Lett.* **100** 056602
- [4] Bernevig B A and Zhang S C 2006 *Phys. Rev. Lett.* **96** 106802
- [5] Maier L, Bocquillon E, Grimm M, Oostinga J B, Ames C, Gould C, Brüne C, Bühhmann H and Molenkamp L W 2015 *Phys. Scr.* **T164** 014002
- [6] Kane C L and Hasan M Z 2010 *Rev. Mod. Phys.* **82** 3045
- [7] Qi X L and Zhang S C 2011 *Rev. Mod. Phys.* **83** 1057
- [8] Schnyder A, Ryu S, Furusaki A and Ludwig A 2008 *Phys. Rev. B* **78** 195125
- [9] Yang Y, Chen S and Li X B 2018 *Acta Phys. Sin.* **67** 237101 (in Chinese)
- [10] Fidkowski and Lukasz 2010 *Phys. Rev. Lett.* **104** 130502
- [11] Hafezi M, Mittal S, Fan J, Migdall A and Taylor J M 2013 *Nat. Photon.* **7** 1001
- [12] Wang Z, Chong Y, Joannopoulos J D and Soljačić M 2009 *Nature* **461** 772
- [13] Poo Y, Wu R X, Lin Z, Yang Y and Chan C T 2011 *Phys. Rev. Lett.* **106** 093903
- [14] Chen W J, Jiang S J, Chen X D, Zhu B, Zhou L, Dong J W and Chan C T 2014 *Nat. Commun.* **5** 5782
- [15] Peano V, Brendel C, Schmidt M and Marquardt F 2015 *Phys. Rev. X* **5** 031011
- [16] Lu L, Joannopoulos J D and Soljačić M 2014 *Nat. Photon.* **8** 821
- [17] Chan H C and Guo G Y 2018 *Phys. Rev. B* **97** 045422
- [18] Ni X, He C, Sun X C, Liu X P, Lu M H, Feng L and Chen Y F 2015 *New J. Phys.* **17** 053016
- [19] Yang Z, Gao F, Shi X, Lin X, Gao Z, Chong Y and Zhang B 2015 *Phys. Rev. Lett.* **114** 114301
- [20] Lu J, Qiu C, Ye L, Fan X, Ke M, Zhang F and Liu Z 2017 *Nat. Phys.* **13** 369
- [21] Vila J, Pal R K and Ruzzene M 2017 *Phys. Rev. B* **96** 134307
- [22] Yang Y, Yang Z and Zhang B 2018 *J. Appl. Phys.* **123** 091713
- [23] Geng Z G, Peng Y G, Shen Y X, Zhao D G and Zhu X F 2018 *Appl. Phys. Lett.* **113** 033503
- [24] Dai H, Xia B and Yu D 2017 *J. Appl. Phys.* **122** 065103
- [25] Dai H, Jiao J, Xia B, Liu T, Zheng S and Yu D 2018 *J. Phys. D-Appl. Phys.* **51** 175302
- [26] Xia B Z, Liu T T, Huang G L, Dai H Q, Jiao J R, Zang X G and Liu J 2017 *Phys. Rev. B* **96** 094106
- [27] Xia B, Fan H and Liu T 2019 *Int. J. Mech. Sci.* **155** 197
- [28] Xia B Z, Zheng S J, Liu T T, Jiao J R, Chen N, Dai H Q and Liu J 2018 *Phys. Rev. B* **97** 155124
- [29] Zhang X, Wang H X, Lin Z K, Tian Y, Xie B, Lu M H and Jiang J H 2019 *Nat. Phys.* **15** 582
- [30] Li Y and Mei J 2015 *Opt. Express* **23** 12089
- [31] Li Y, Wu Y and Mei J 2014 *Appl. Phys. Lett.* **105** 014107
- [32] Mei J, Wu Y, Chan C T and Zhang Z Q 2012 *Phys. Rev. B* **86** 035141
- [33] Wu Y 2014 *Opt. Express* **22** 1906
- [34] Lu J, Qiu C, Xu S, Ye Y, Ke M and Liu Z 2014 *Phys. Rev. B* **89** 134302